74th International Astronautical Congress (IAC), Baku, Azerbaijan, 2-6 October 2023.

IAC-23-C1.6.1

Design of optimal spatial low-energy trajectories to Near Earth Objects

David Canales[a], Elena Fantino[b], Katleen C. Howell[c], R. Flores[d]

[a] *Department of Aerospace Engineering, Embry–Riddle Aeronautical University, Daytona Beach, FL 32117, USA,* canaled4@erau.edu
[b] *Department of Aerospace Engineering, Khalifa University of Science and Technology, P.O. Box 127788, Abu Dhabi, United Arab Emirates,* elena.fantino@ku.ac.ae
[c] *School of Aeronautics and Astronautics, Purdue University, West Lafayette, IN 47907, USA,* howell@purdue.edu
[d] *Department of Aerospace Engineering, Khalifa University of Science and Technology, P.O. Box 127788, Abu Dhabi, United Arab Emirates,* robertomaurice.floresleroux@ku.ac.ae

Abstract

Near Earth Objects (NEOs) are small Solar System bodies (such as asteroids, comets and meteoroids) in heliocentric orbits with perihelion below 1.3 astronomical units. With a catalog of over 30,000 known asteroids and approximately 100 listed short-period comets, the NEO population represents an inventory of exploration targets reachable with significantly lower cost than the objects of the Main Asteroid Belt. Similarly to the latter, NEOs are primordial bodies, hence their study can provide insight into the origins of our planetary system. In addition, the materials present in these objects can be used to resupply spacecraft on course to other destinations. Past missions to NEOs, such as NEAR, Hayabusa, ICE, and Deep Impact, have traditionally used the patched-conics approximation, often combined with impulsive and/or low-thrust maneuvers. This contribution builds on a previous work which proposed a novel design technique that leverages the invariant dynamical structures of the planar circular restricted three-body problem (CR3BP) and the efficiency of the Keplerian approximation to connect the vicinity of the Earth with NEOs in nearly circular, low-inclined heliocentric orbits through planar Lyapunov orbits around the collinear points L_1 and L_2 of the Sun-Earth CR3BP. The resulting trajectories follow low-energy paths; therefore, they naturally minimize the launch cost. In this contribution, we develop an extension of the technique to the 3D domain, using libration point orbits with their hyperbolic invariant manifolds and an adaptation of a trajectory design method called MMAT to approach NEOs on inclined orbits. We evaluate key parameters such as time of flight, launch energy and ΔV to perform rendezvous with a variety of targets, and compare our results with existing solutions and past missions. Finally, we present a methodology to reshape the rendezvous maneuver using low-thrust arcs.

Keywords: Near Earth Objects; spacecraft trajectories; three-body problem; impulsive maneuvers; low-thrust transfers

1. Introduction

Near Earth Objects (NEOs) are asteroids (NEAs) and comets (NECs) with perihelion below 1.3 au [1]. Notable efforts have been devoted to studying NEOs because scientists believe that their characterisation is key to deepening our understanding of the origin and evolution of the Solar System and the source of water on Earth. These bodies have also received attention because of their proximity to Earth, which is often associated with collision threats. Lastly, in recent years, NEOs have gained importance in the context of resource utilization, a practice encouraged by the idea that the in-situ collection and storage of resources available in space will help lower the cost of space missions.

The first spacecraft (S/C) to visit a NEO was NASA's NEAR Shoemaker which landed on the surface of 433 Eros in 2001 [2]. This endeavour was followed by the planned collision of NASA's Deep Impact with comet Tempel 1 in 2005 [3]. In the same year, JAXA successfully completed a sample return mission to asteroid Itokawa with the Hayabusa S/C [4], whereas in 2010, the Deep Impact's mission extension called EPOXI carried out a flyby with comet Hartley 2. In 2012, CNSA's Change'e 2 executed a close approach with 4179 Toutatis [5]. Between 2018 and 2020, JAXA's follow-up mission Hayabusa 2 rendezvoused with asteroid Ryugu, collected samples of its surface and returned them to Earth [6]. The S/C is now on an extended mission to asteroid 1998 KY26. NASA's OSIRIS-Rex [7] successfully rendezvoused with Bennu, touched down on its surface and extracted samples that will be delivered to Earth in September 2023. The probe will then continue its journey to encounter and study 99942 Apophis in 2029. The Double Asteroid Redirection Test (DART [8]) conducted by NASA aimed at demonstrating a method for planetary defense. In 2022, DART collided with Dimorphos and shortened the orbit of this body by 32 minutes, proving the effectiveness of the transfer of momentum from the S/C to the asteroid. The trajectories of these probes were designed using patched-conics, gravity assists and impulsive or

continuous-thrust maneuvers, and were characterized by mission durations ranging from 100 days to a few years and close-approach speeds relative to the target between 10 m/s and 10 km/s.

A number of studies (see e.g., [9,10,11,12]) have proposed methods to rendezvous, retrieve and transport portions or entire asteroids to near-Earth space. The trajectory design techniques include conventional patched conics, direct Lambert arcs, gravity-assisted trajectories as well as invariant manifold orbits, and employ high-thrust (HT) or low-thrust (LT) propulsion. Human exploration of NEAs has gained a lot of interest too. Since 2012, NASA has been updating the Near-Earth Object Human Space Flight Accessible Target Study (NHATS) list [13] that contains targets on orbits very close to Earth's and reachable by a round-trip mission of a limited duration. The trajectory design is carried out with the method of patched conics, and employs full precision JPL ephemerides for both the S/C and the asteroids.

The approach proposed in this work leverages the dynamical properties of the invariant structures of the circular restricted-three body problem (CR3BP) with the objective of lowering the launch and transfer costs to NEOs on orbits close to Earth's. In its current form, the technique allows for rendezvous with NEOs using low-energy trajectories associated with planar periodic orbits around the collinear libration points L_1 and L_2 of the Sun-Earth CR3BP. The key feature of the method is the approximation of the three-body orbit of the S/C with a Keplerian (two-body, 2BP) ellipse at a sufficient distance from the Earth, a strategy also called patched CR3BP/2BP model (see also [14, 15]). Thus, the rendezvous problem is solved through the calculation of intersections between confocal heliocentric ellipses, i.e., the orbit of the S/C and the target NEO. In addition, since the former is generated in the Sun-Earth synodic barycentric reference frame, the orientation in space of the heliocentric ellipse depends on the departure epoch and varies linearly with it. This element constitutes a degree of freedom of the model and facilitates the selection of the most desirable solutions (e.g., low transfer impulse ΔV, low transfer time Δt). The motion of the S/C is associated with planar Lyapunov orbits (PLOs) around L_1 or L_2 either through trajectories of the unstable hyperbolic invariant manifolds (UHIMs) of these orbits or in the form of transit orbits (TOs). Impulsive maneuvers or equivalent LT transfers cause the S/C to rendezvous with the target at zero relative speed. The methodology has been developed in the planar approximation for low-inclination targets whose orbits are projected on the ecliptic plane, and subsequently has been extended to spatial (3D) solutions.

The paper starts with the illustration of the dynamical model of the S/C (Sect. 2), the selection of the target NEOs and the computation of their trajectories (Sect. 3). Sections 4 to 6 present the methodology and the results for planar impulsive (Sect. 4) and LT (Sect. 5) transfers, and spatial impulsive (Sect. 6) solutions. Section 7 illustrates the strategy designed to compute LT rendezvous trajectories in 3D. Section 8 concludes the paper.

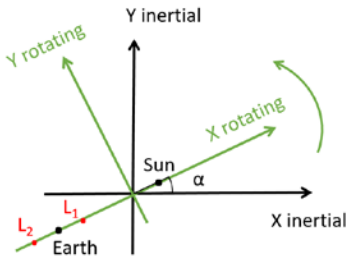

Figure 1: The Sun-Earth synodic barycentric reference frame (rotating axes), the barycentric ecliptic J2000.0 reference frame (inertial axes), the Sun, the Earth and the two collinear equilibrium points L_1 and L_2.

2. S/C dynamical model

In the vicinity of the Earth, the S/C moves under the gravitational attraction of both the Sun (mass M_*) and the Earth (mass M_+), assumed to follow circular orbits around their center of mass. The equations of motion of the S/C are expressed in the synodic barycentric reference frame of the primaries, with these two bodies on the x axis [16] (Fig. 1), the Sun at (μ,0,0) and the Earth at (μ-1,0,0), μ being the mass ratio $M_+/(M_++M_*)$ of the system. Using the gravitational constant G, the sum M_++M_* of the masses and the distance d between the primaries as reference magnitudes, the mean motion of the orbits of the primaries takes unitary value and their orbital period equals 2π. Table 1 lists the relevant physical and dynamical parameters of the Sun-Earth system.

Table 1. Patched CR3BP/2BP: relevant physical and orbital parameters [18].

Symbol	Definition	Value	Units
GM_*	Sun's gravit. parameter	$1.3271244 \cdot 10^{11}$	km^3/s^2
GM_+	Earth's gravit. parameter	$3.9860044 \cdot 10^5$	km^3/s^2
R_+	Earth's equat. radius	6378.1366	km
μ	Earth-Sun mass ratio	$0.30034806 \cdot 10^{-5}$	-
d	Earth-Sun distance	149597870.700	km

Figure 2 illustrates families of PLOs around the two collinear equilibrium points L_1 and L_2. Each set contains 50 orbits equally spaced in Jacobi constant C_J, approximately ranging from 3.00058 (y amplitude of $3 \cdot 10^6$ km) to 3.00089 (y amplitude of $9 \cdot 10^3$ km).

The PLOs are employed to generate two types of trajectories for the S/C:

- Outward branches of UHIMs (200 trajectories for each PLO), determined and propagated using standard methods, i.e., an initial state is generated by applying a small perturbation in the outward direction of the unstable eigenvector of the monodromy matrix of the PLO after appropriate time transformation through the state transition matrix (see e.g., [17]); this is followed by globalization of the manifold by propagation forward in time.
- TOs, obtained by discretizing the area encircled by a PLO with a grid (originally 70 x 70 points forming a rectangular area bounding the PLO, see Fig. 3); each point internal to the PLO is the initial position of a TO with the same C_J value as the PLO, while the direction of the velocity is set either parallel (L_1) or anti-parallel (L_2) to the x axis. TOs drive the S/C away from the Earth forward in time following paths contained within the outward UHIM branch with the same C_J.

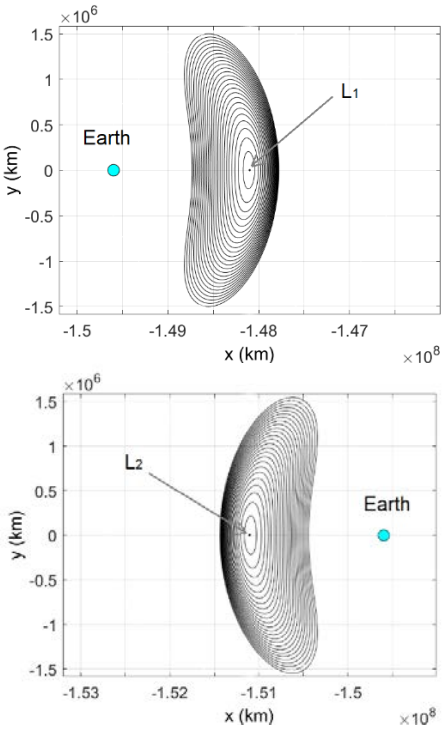

Figure 2: The families of PLOs around L_1 (top) and L_2 (bottom).

The initial states of the TOs are propagated backwards in time (i.e., towards the Earth). The trajectories that cross a given circular parking orbit (in this study at an altitude of 300 km above the surface of the Earth) are retained, the others are discarded (Fig. 4).

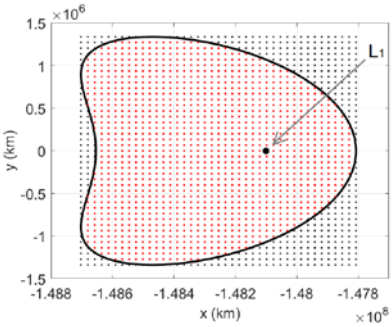

Figure 3: Generation of the grid of points internal to a PLO around L_1, sources of the TOs.

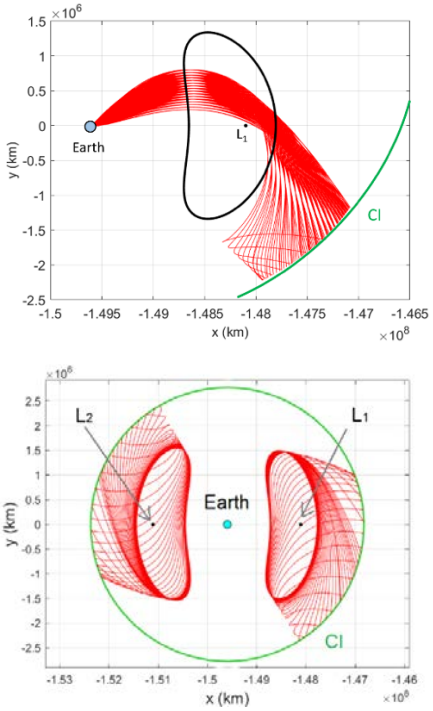

Figure 4: Propagation of a set of TOs (top) and outward branches of two UHIMs (bottom) to the CI.

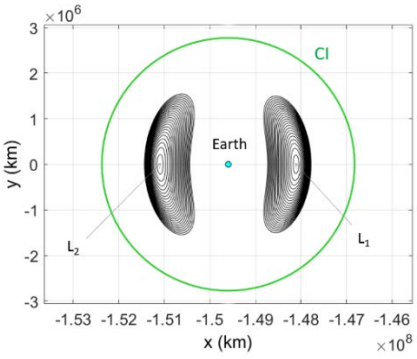

Figure 5: The CI and the orbits of the two families.

The selected TOs and all the UHIMs are propagated forward in time until they intersect an Earth-centered circle, called circle of influence (CI, Fig. 4) whose radius r_{CI} equals that of the Laplace sphere of influence of the Earth $d\ (M_+/M_*)^{2/5}$ scaled by a factor 3, so as to make it

sufficiently large to encircle all the PLOs of the two families (Fig. 5).

The state vectors of UHIMs and TOs at the CI are then transformed to the heliocentric ecliptic J2000 reference frame and propagated in the Sun-S/C 2BP (in this operation, the distance between the barycentre of the Sun-Earth system and the center of the Sun is neglected). The transformation is time dependent, i.e., it depends on the angle that the *x* axis of the synodic frame forms with the inertial frame at the time of CI crossing. This affects the orientation in space (longitude of perihelion) of the osculating heliocentric ellipse of the S/C, whereas semimajor axis, eccentricity, inclination and true anomaly are entirely determined by the state at the CI in the synodic frame.

UHIMs trajectories depart from the respective initial conditions close to the progenitor PLOs, whereas TOs start at their intersection points with the LEO orbit. In both cases, the same reference departure epoch 2460000.5 JD is assigned to all initial states. Due to the above mentioned time-varying orientation of the osculating ellipse, the actual individual departure date for each trajectory is defined *a posteriori* on the basis of the rendezvous requirements.

The propellant budget of transfers that employ impulsive maneuvers is computed assuming a chemical propulsion system with a specific impulse I_{sp} of 300 s, whereas for the LT solutions, I_{sp} = 3100 s and the thrust T is set at 80 mN. The launch mass m_0 of the S/C is 1000 kg. In the LT case, the mass is kept constant over the transfer, leading to a conservative value of $8 \cdot 10^{-5}$ m/s^2 for the acceleration throughout the flight.

3. NEOs database and dynamical model

The candidate targets for the rendezvous simulations have been selected from the Solar System Dynamics minor bodies database [19]. The available NEOs have been filtered on the basis of their inclination (less than 5 degrees with respect to the ecliptic plane) and their perihelion and aphelion distances (greater than 0.9 au and lower than 1.1 au, respectively). This has yielded a set of 72 asteroids and 0 comets (their orbits are shown in Fig. 6). In the subsequent computations, their orbital elements (ecliptic Sun-centered J2000.0) at the osculating epoch (2460000.5 JD for all the objects) have been used as initial conditions for the propagation of the state of each object in the heliocentric 2BP.

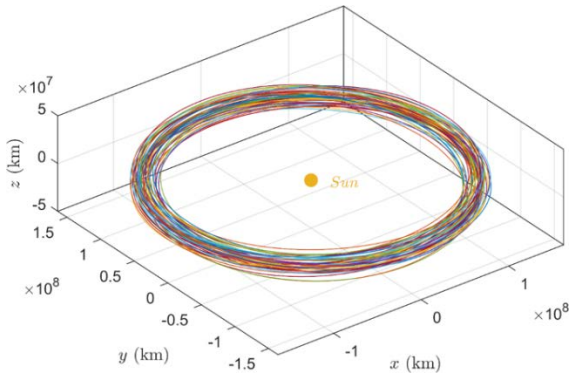

Figure 6: 2BP orbits of the selected NEOs.

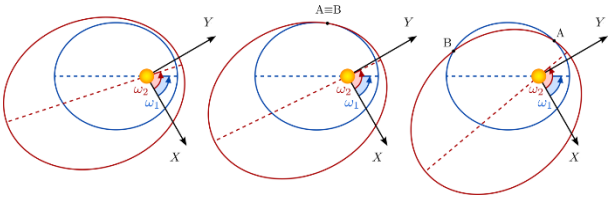

Figure 7: Variation of the number of intersections (0 on the left, 1 in the middle, 2 on the right) between confocal coplanar ellipses as a function of their relative orientation, expressed as the difference between the respective pericenter longitudes ω_1 and ω_2.

4. Planar impulsive rendezvous

Neglecting the gravitational attraction of the Earth outside the CI transforms the design of a transfer to a NEO into the search for intersections between confocal ellipses. In the planar approximation, the selected low-inclination targets are assumed to orbit on the ecliptic plane (their orbital inclination is neglected), whereas the S/C moves on the ecliptic by construction. Hence, the rendezvous with a given NEO occurs at the intersection (if any) between two coplanar confocal elliptical orbits. The solution of this mathematical problem is due to [20] and was recently applied by [14, 15, 21, 22] to the case of transfers between giant planet moons. The values of semimajor axis and eccentricity of the orbits of the two bodies determine whether their paths intersect and for which values of the angle between the respective periapses (see Fig. 7). The longitude of the perihelion of the orbit of the NEO is considered fixed, whereas in the case of the S/C this quantity is a function of the CI crossing date, which, for a given UHIM trajectory or TO depends on the departure epoch. The freedom on the choice of the departure date is a consequence of the autonomous character of the CR3BP. Two confocal coplanar ellipses admit at most two intersection points. When the orbits intersect tangentially, these points coincide and yield the minimum velocity difference ΔV at an intersection between the two ellipses (see Fig. 7).

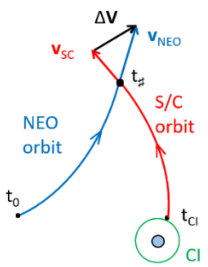

Figure 8: The position of the rendezvous point determines the encounter date $t_\sharp$ and this, in turn, determines the date of CI crossing t_{CI} for the S/C.

The range of values of the longitude of the perihelion of the orbit of the S/C for which intersections with the target NEO orbit exist is identified and then discretized (step $\Delta\omega$). Each value in the set (called desired ω) is used to determine the position of the intersection point(s) between the two elliptical orbits. The transfer time of the target NEO from the osculating epoch t_0 to an encounter point yields an encounter date $t_\sharp$, which in turn provides the desired date t_{CI} of CI crossing for the S/C (Fig. 8). This date is associated with a specific value of the longitude of the perihelion, called real ω. In general, desired ω and real ω do not coincide. However, also in virtue of the above discretization, a small difference between them is admissible. This discrepancy ω_{err} translates into a non-zero minimum distance $\Delta r_\sharp$ between the S/C and the target at $t_\sharp$. The size of $\Delta r_\sharp$ depends on ω_{err}, on the distance of the encounter point from the CI and the eccentricity of the two orbits. It can be eliminated by applying a correction maneuver, for example by solving Lambert's problem between CI crossing position and rendezvous point. In this way, the transfer involves two impulses, instead of one. Alternatively, $\Delta r_\sharp$ can be reduced or eliminated by replacing the impulsive rendezvous maneuver with a LT transfer, as illustrated in Sect. 5.

Table 2. Simulation parameters for 2D impulsive transfers (discretization interval $\Delta\omega$, maximum allowed difference ω_{err} between real and desired ω, maximum allowed impulse ΔV at rendezvous) and number of solutions obtained for each combination of trajectory type and libration point.

	$\Delta\omega$ (degree)	ω_{err} max. (degree)	ΔV max. (m/s)	Number of sols. -
UHIM L_1	0.2	0.02	500	1285
UHIM L_2	0.1	0.01	230	2190
TO L_1	0.2	0.04	500	740
TO L_2	0.1	0.01	250	3539

The parameters of the simulations are listed in Table 2, which also reports the number of solutions obtained for each trajectory type and libration point. Table 3 summarizes the main features of the solutions obtained with the parameter values of Table 2: for each combination of trajectory type and libration point, the table provides the primary designations of the NEOs that the S/C can encounter and indicates the minimum rendezvous impulse, the corresponding propellant mass consumption, the minimum close approach distance and the minimum transfer time from the PLO (for UHIMs) or from LEO (in the case of TOs) to each accessible NEO. The top panels of Figures 9-11 illustrate the solutions for the three cases labelled (a), (b) and (c) in Table 3.

Table 3. Primary designations of the accessible NEOs and the solutions with minimum rendezvous impulse, minimum close approach distance and minimum transfer time from the PLO (for UHIMs) or from LEO (in the case of TOs).

	Primary design.	ΔV min. (m/s)	(Δm) (kg)	$\Delta r_\#$ min. (km)	Δt min. (day)
UHIM L_1	2018 PN_{22}		355 (114)	153	354.5
	2020 HO_5		405 (129)	11	485.6
	2020 VN_1	(a)	467 (147)	495	436.5
	2021 GM_1		327 (105)	158	577.1
UHIM L_2	2022 NX_1		133 (44)	7	445.6
	2022 RD_2		132 (44)	74	(c) 419.3
	2022 RW_3		153 (51)	30	510.5
	2023 GT_1		133 (44)	176	316.1
TO L_1	2018 PN_{22}		418 (132)	1973	290.8
	2020 HO_5		406 (129)	67	390.8
	2020 VN_1		466 (146)	5575	355.8
TO L_2	2022 NX_1		131 (44)	194	317.0
	2022 RD_2		135 (45)	(b) 739	330.3
	2022 RW_3		172 (57)	259	330.5
	2023 GT_1		132 (44)	21	107.6

5. Planar low-thrust trajectories

The impulsive maneuver at rendezvous and any residual distance between the S/C and the target at $t_\sharp$ can be eliminated by introducing one or more low-thrust arcs. The method developed in this work applies thrust only outside the CI and preserves the event dates (t_{CI}, $t_\sharp$) and the S/C position at CI crossing, as determined in the impulsive case. The interval $t_\sharp$ - t_{CI} is discretized into n steps Δt_i (i = 1, 2, …, n, with n sufficiently large, for example n = 1000 for a transfer time of 100 days) and the trajectory of the S/C is propagated backwards in time from $t_\sharp$ by imposing that the state $\mathbf{s}_\sharp$ = ($\boldsymbol{r}_\sharp$,$\boldsymbol{v}_\sharp$) at $t_\sharp$ coincides with that of the target NEO $\boldsymbol{s}_{NEO}$ = ($\boldsymbol{r}_{NEO}$, $\boldsymbol{v}_{NEO}$), thus ensuring rendezvous at zero relative speed and distance. During step i (which occurs between times t_i and t_{i-1}, with i ranging from n to 2), thrust is applied in the fixed direction $\boldsymbol{u}_i$. This direction is chosen to minimize the sum of the magnitudes ΔV_{i1} and ΔV_{i2} of the two impulses needed for a ballistic transfer between $\boldsymbol{r}_{CI}$ (position at CI crossing, where the velocity is $\boldsymbol{v}_{CI}$) and $\boldsymbol{r}_{i-1}$ (position at t_{i-1} where the velocity is $\boldsymbol{v}_{i-1}$). Refer to Fig. 12, where the velocities at the end points of the ballistic arc are labeled $\boldsymbol{v}_{i1B}$ and $\boldsymbol{v}_{i2B}$. The propagation is carried out by numerically integrating the equations of motion:

$$\frac{\mathrm{d}^2\mathbf{r}}{\mathrm{d}t^2} = -\frac{GM_\star}{r^3}\mathbf{r} + \frac{T}{m_0}\mathbf{u}_i. \qquad (1)$$

The process is iteratively applied across all steps, leading to a transfer where the initial rendezvous impulse is offset by continuous thrust. This method maintains the initial state, the rendezvous point (NEO position at $t_\sharp$), and the duration of the original impulsive trajectory (i.e., time interval between t_{CI} and $t_\sharp$).

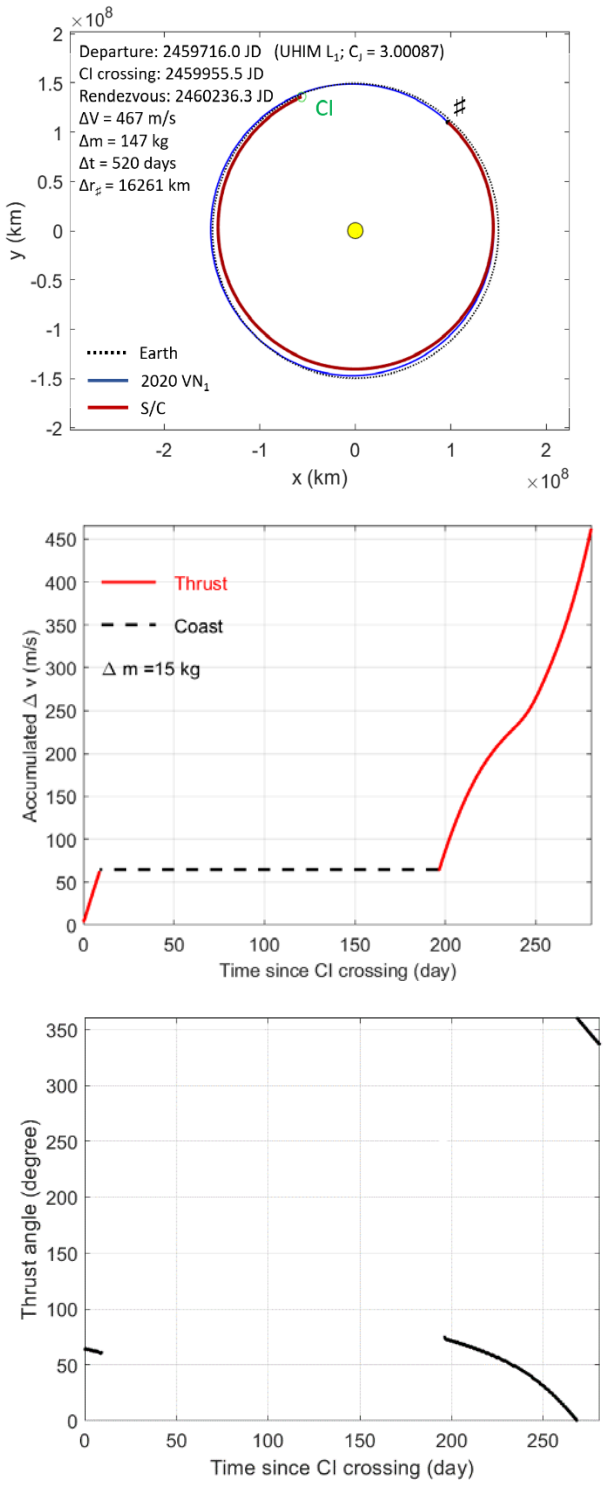

Figure 9: Case (a) from Table 3. Top: trajectories of S/C, Earth and NEO and transfer details for the impulsive solution. Middle and bottom: ΔV decrease profile and thrust angle with respect to the local circumferential direction for the low-thrust version.

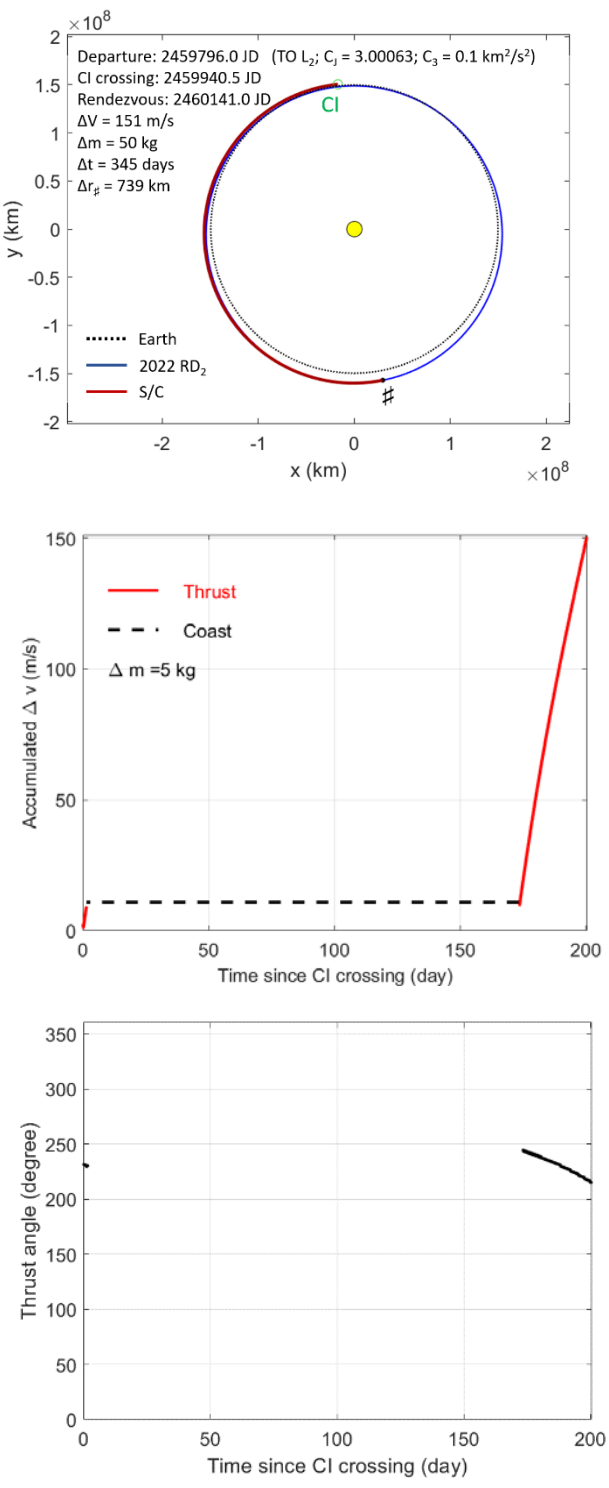

Figure 10: Case (b) from Table 3. Top: trajectories of S/C, Earth and NEO and transfer details for the impulsive solution. Middle and bottom: ΔV decrease profile and thrust angle with respect to the local circumferential direction for the low-thrust version.

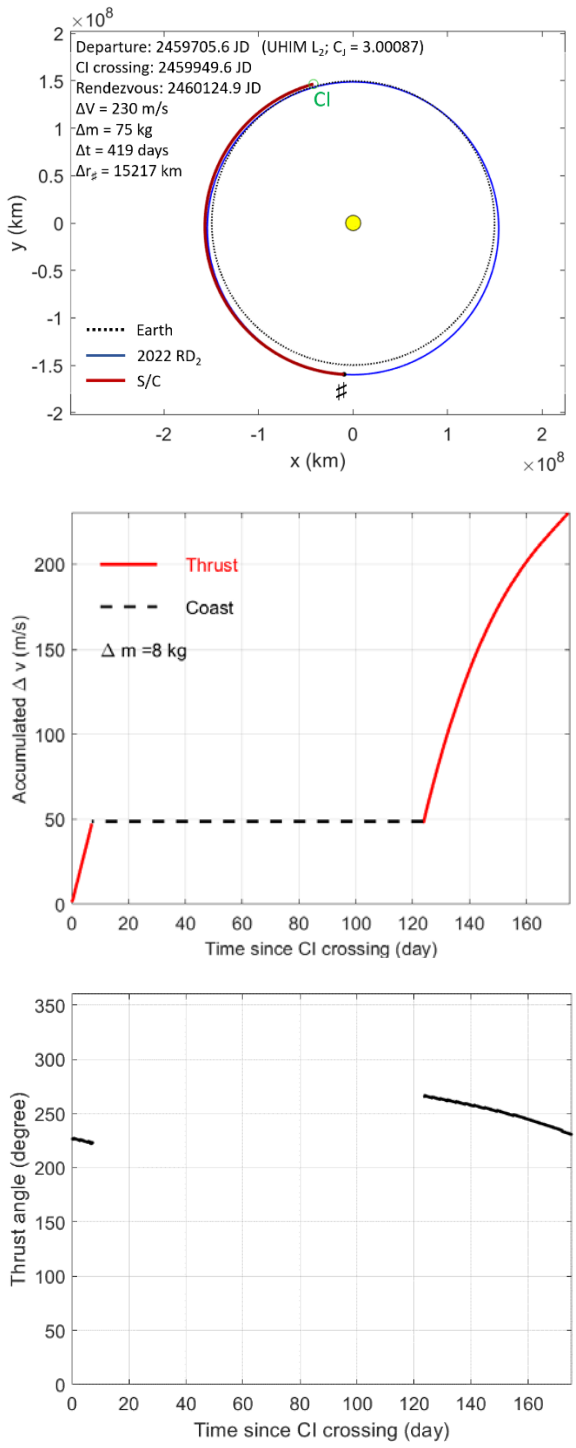

Figure 11: Case (c) from Table 3. Top: trajectories of S/C, Earth and NEO and transfer details for the impulsive solution. Middle and bottom: ΔV decrease profile and thrust angle with respect to the local circumferential direction for the low-thrust version.

However, the function $f(\boldsymbol{u}_i) = \Delta V_{i1} + \Delta V_{i2}$ may reach a local minimum after some steps, preventing the process to compensate the total impulse. When this happens (e.g., at step j, where the state is $\boldsymbol{s}_j = (\boldsymbol{r}_j, \boldsymbol{v}_j)$ thrusting is interrupted. The propagation is resumed forward in time from $\boldsymbol{s}_{CI} = (\boldsymbol{r}_{CI}, \boldsymbol{v}_{CI})$ to step j-1. At each intermediate step $k = 1, 2, \ldots, j$-1, thrust is applied in the direction $\boldsymbol{u}_k$ that minimizes the sum of the magnitudes ΔV_{k1} and ΔV_{k2} for the two impulses required to execute a ballistic arc between position $\boldsymbol{r}_{k+1}$ at the end of step k (velocity $\boldsymbol{v}_{k+1}$) and $\boldsymbol{r}_{j-1}$ (velocity $\boldsymbol{v}_{j-1}$). This is illustrated in Fig. 13, where the velocities at the endpoints of the ballistic arc are denoted $\boldsymbol{v}_{k1B}$ and $\boldsymbol{v}_{k2B}$.

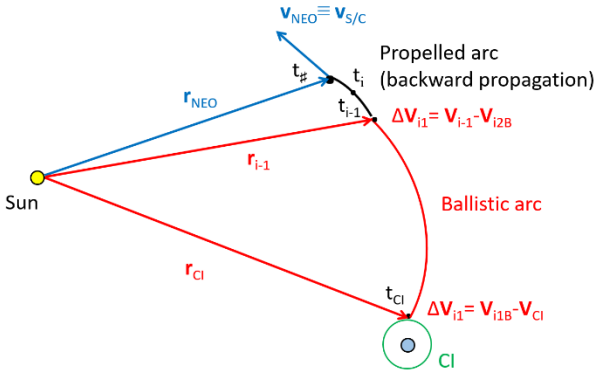

Figure 12: Backward trajectory propagation with thrust.

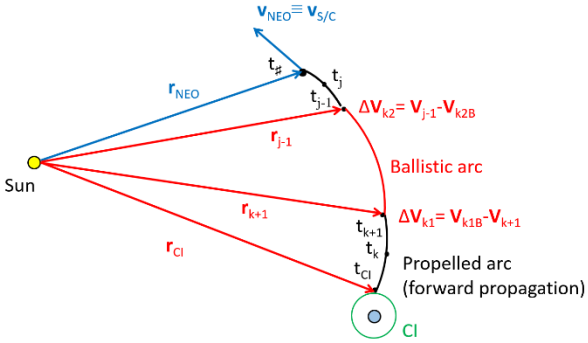

Figure 13: Forward trajectory propagation with thrust.

The middle and bottom panels of Figs. 9-11 show the performance of the LT solutions for cases (a), (b) and (c) of Table 3: the history of the accumulated imparted ΔV, and the direction of thrust, represented by the angle that $\boldsymbol{u}$ forms with the local circumferential direction. All three trajectories are of type thrust-coast-thrust, and the total ΔV provided by the engine is very close to the value of the original impulsive solution.

6. Spatial impulsive trajectories

The planar approximation should only be applied when the target's orbital inclination is very small. In fact, also for the low-inclination targets considered in this work, neglecting the velocity variation associated to the change of plane may lead to a non-realistic assessment of the propellant budget and the rendezvous date.

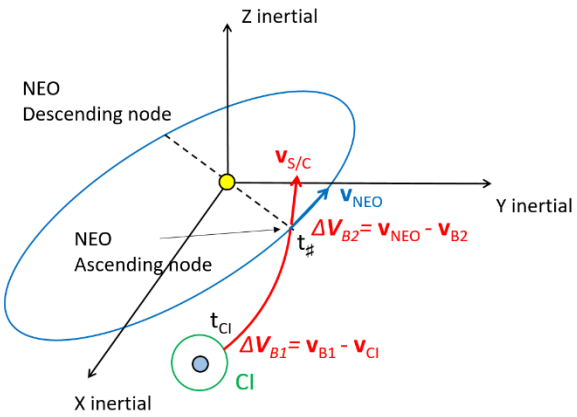

Figure 14: 3D impulsive transfer from CI exit to the ascending node of the orbit of the target NEO.

Table 5. Primary designations of the accessible NEOs, number of solutions, and 3D impulsive trajectories with minimum total impulse (and propellant consumption), minimum close approach distance and minimum transfer time from the PLO (for UHIMs) or from LEO (in the case of TOs).

	Primary design.	# of sols.	ΔV min. (m/s)	(Δm) (kg)	Δt min. (day)
UHIM L_1	2021 GM_1	712	1303	(358)	535.3
	2022 NX_1	3748	1183	(331)	468.9
	2022 RD_2	407	1321	(362)	481.0
	2023 FY_3	1546	1127	(318)	417.6
	2023 HG_{11}	197	1267	(350)	454.2
UHIM L_2	2011 MD	953	1397	(378)	248.5
	2019 GF_1	1230	1241	(344)	322.0
	2021 GM_1	352	1460	(391)	409.5
	2022 NX_1	253	1286	(354)	540.3
	2022 RD_2	966	1272	(351)	260.3
	2023 FY_3	5	1313	(360)	249.0
	2023 HG_{11}	607	(*) 697	(211)	455.4
TO L_1	2020 WY	1	1359	(370)	65.3
	2021 GM_1	7	1415	(382)	442.0
	2022 NX_1	744	1210	(337)	278.5
	2022 RD_2	295	1336	(365)	303.9
	2023 FY_3	798	1196	(334)	230.0
	2023 HG_{11}	537	1287	(354)	254.2
TO L_2	2019 GF_1	15	1278	(352)	320.8
	2022 NX_1	1954	(**) 582	(180)	238.7
	2022 RD_2	1954	742	(223)	292.8
	2023 FY_3	1942	998	(288)	87.7
	2023 HM_4	157	1107	(313)	121.4
	2023 HG_{11}	1954	653	(199)	242.9

Impulsive spatial transfers taking into account the 3D orientation of the orbits of the candidate NEOs have been computed in this work by analyzing the spatial intersections between confocal non-coplanar elliptical orbits when one (NEO) is fixed in space whereas the other (S/C) lies on the ecliptic plane and its longitude of the perihelion depends on the date of CI crossing. The intersection between the two ellipses can only occur at either node of the target body's orbit. While yielding two geometric solutions, temporal alignment is not guaranteed (Sect. 4). Conversely, the nodes of the orbit of the target body are the rendezvous points with the lowest transfer ΔV. For this reason, the chosen approach involves adjusting the CI crossing date (and the departure date accordingly) to calculate the ballistic heliocentric transfer between CI and either target's node. The computation of such Lambert arc yields two impulses, one at the CI in the ecliptic plane, and one at the rendezvous point in 3D (see Fig. 14).

The simulations have been carried out for both types of trajectories (UHIMs and TOs) using a discretization of 5 days for the CI crossing date and capping the solutions to 1500 m/s of total ΔV. The results obtained are summarized in Table 5, which for each accessible target and S/C trajectory type lists the number of available trajectories, the solution with the minimum total cost and the fastest transfer. Figures 15 and 16 illustrate the ecliptic projection and the 3D view of the transfers labelled with (*) and (**) in Table 5.

7. Extension to spatial low-thrust trajectories

The planar approach is extended to 3D with minor changes, by performing the maneuver in two distinct steps. First, a change of plane applying thrust along the direction of the orbital angular momentum. This stage adjusts the orbit's inclination and longitude of the ascending node to match those of the target. The second step is a planar rendezvous using the strategy described in Sect. 5. The date of departure from Earth is no longer a free parameter; it is determined by the duration of the plane change step and the longitude of the ascending node of the asteroid. The maneuver requires cycling the thrust between parallel and anti-parallel to the angular momentum vector (otherwise, the inclination would oscillate instead of growing monotonically). The direction switch takes place when the orbital angular momentum, the pole of the ecliptic and the heliocentric position vector become coplanar (i.e., approximately once each half-revolution around the Sun). Figure 17 shows the evolution of inclination for a target inclined 4.7 degrees relative to the ecliptic. The horizontal points of the curve coincide with the thrust reversals. With this strategy, the phasing between the target and the S/C once the target plane is reached is determined by the Earth departure conditions and the plane change maneuver. Thus, the relative phase can be very different from the planar case, resulting in excessive impulse requirements. There are two simple ways to mitigate this issue. One is testing different sets of departure conditions in order to determine which one yields the lowest impulse. The other is to take advantage of the small slope of the inclination curve in the neighborhood of the points where the thrust reverses. There is a window of approximately two months where the control strategy can be changed with minimal impact on the duration of the maneuver and propellant consumption. It is then possible to apply thrust in the tangential direction. This would change the semimajor axis and, consequently, the orbital period, allowing control over the relative phase at the end of the plane change.

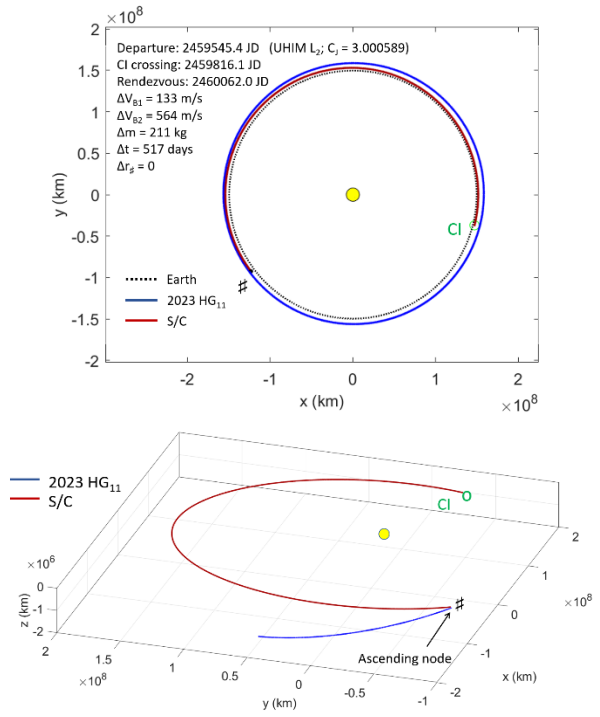

Figure 15: Ecliptic projection (top) and 3D view (bottom) of the transfer with the lowest total impulse from a UHIM trajectory around L_2 to the ascending node of the orbit of 2023 HG_{11} target inclination = 2 degrees).

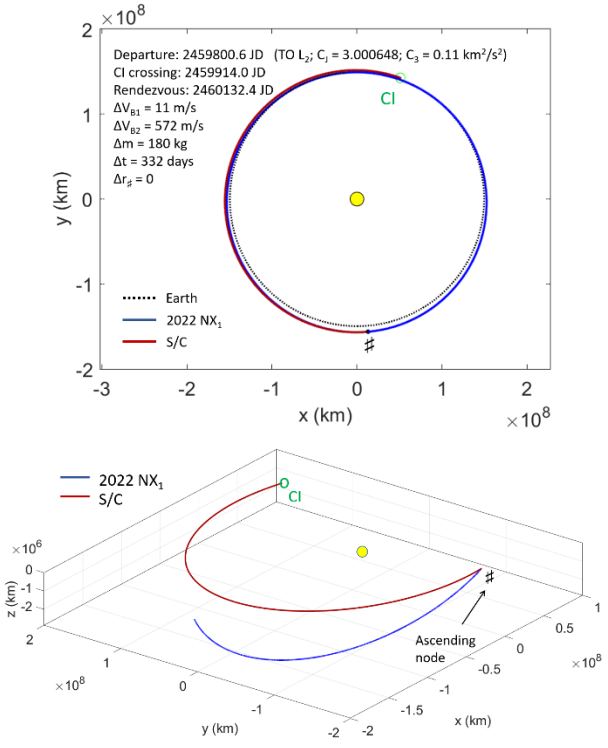

Figure 16: Ecliptic projection (top) and 3D view (bottom) of the transfer with the lowest total impulse from a TO trajectory around L_2 to the ascending node of the orbit of 2022 NX_1 target inclination = 1 degree).

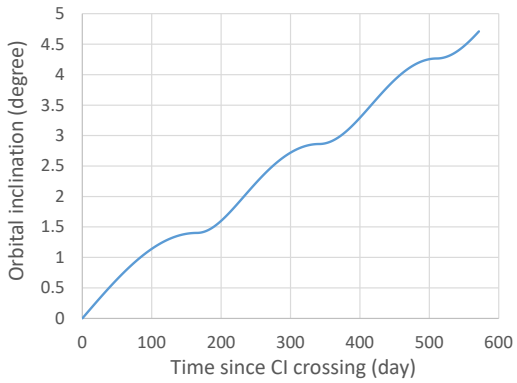

Figure 17: Evolution of inclination during change of plane maneuver. Average inclination rate is 0.25 degree/month.

8. Discussion and conclusions

The present contribution is a preliminary analysis of the transfer opportunities offered by the invariant dynamical structures of the Sun-Earth CR3BP to reach selected NEOs. The study shows that departing from a planar Lyapunov orbit around a collinear libration point or from a LEO parking orbit and moving on hyperbolic invariant manifold trajectories or transit orbits is beneficial in terms of launch cost, impulse of the rendezvous maneuver and time of flight.

For targets with low-inclination orbits relative to the ecliptic, the transfers have been computed in a planar approximation (both the S/C and the NEO are assumed to orbit on the ecliptic) as well as in 3D (i.e., taking into account the spatial orientation of the orbit of the NEO). Following a methodology previously applied to trajectories between giant planet moons, the state of the S/C departing Earth on a three-body orbit is used to compute an osculating heliocentric elliptical orbit at the crossing of a suitably-defined sphere of influence (the CI) around the Earth. Such osculating orbit has the advantage that the longitude of its perihelion varies with the CI crossing date. This yields large sets of rendezvous opportunities with the candidate targets in the form of intersection points between their orbits and that of the S/C. In the 2D impulsive case, no maneuver is applied until rendezvous. For targets on low-eccentricity orbits close to that of the Earth, transfer times range between 3 months and 1.5 years, with the impulse at rendezvous in the 100-500 m/s range. Due to the discretization introduced in the search for intersections, the 2D solutions do not bring an exact position match with the target at rendezvous, but such distance can be reduced or eliminated either by applying an additional impulse or by replacing the impulsive strategy with a low-thrust transfer. The latter is implemented in a way that preserves the CI crossing date and state vector as well as the transfer duration, thus allowing a direct comparison between impulsive and continuous-thrust trajectories: the amount of propellant required to complete the same

transfer with electric propulsion is 10% of that associated with a chemical thruster.

Even for low-inclination NEOs, the elevation of the target with respect to the ecliptic plane needs to be considered in order for the trajectories to be realistic. A methodology to compute 3D transfers with impulsive maneuvers has been developed and applied to the same three-body departure conditions studied in the planar case. The state of the S/C at CI crossing still lies on the ecliptic plane, but the orbit of the NEO is considered in 3D, and a Lambert arc is solved between CI crossing position and rendezvous. Varying the CI crossing date and the rendezvous date yields a wide range of transfer ΔVs, which can reach values of several km/s. The cost can be greatly reduced (to 500 m/s in some cases) by requiring that the S/C encounters the NEO at one of the nodes of its orbit. Low-thrust maneuvers have the potential for large efficiency improvements and are currently being investigated. We propose a simple extension of the 2D strategy by introducing an initial change of plane maneuver which adjusts the inclination and longitude of the ascending node. The next step follows closely the planar case, but with the departure date constrained by the requirements of the plane change segment. The 3D low-thrust extension shall enable higher-fidelity benchmarking against alternative mission design strategies found in the literature.

Acknowledgements

E. Fantino and R. Flores acknowledge Khalifa University of Science and Technology's internal award CIRA-2021-65 (8474000413). E. Fantino was also partially supported by grants PID2020-112576GB-C21 and PID2021-123968NB-I00 of the Spanish Ministry of Science and Innovation. R. Flores acknowledges financial support from the Spanish Ministry of Economy and Competitiveness "Severo Ochoa Programme for Centres of Excellence in R&D" (CEX2018-000797-S).

References

[1] Center for Near-Earth Objects Study, NEO Basics, https://cneos.jpl.nasa.gov/about/basics.html (last accessed Aug. 20, 2023)

[2] NASA, NEAR Shoemaker (2021), https://solarsystem.nasa.gov/missions/near-shoemaker/in-depth/ (last accessed Aug. 20, 2023)

[3] NASA, Deep Impact (EPOXI) (2021), https://solarsystem.nasa.gov/missions/deep-impact-epoxi/in-depth/ (last accessed Aug. 20, 2023)

[4] JAXA, Hayabusa arrives at Itokawa (2005), https://www.isas.jaxa.jp/e/snews/2005/0912.shtml (last accessed Aug. 20, 2023)

[5] Liu, L., Lie, Y., Cao, J.-F., et al. (2014): Mission design of the CHANG'E-2 asteroid exploration, *Journal of Astronautics* 35, pp. 262-268. DOI: 10.3873/j.issn.1000-1328.2014.03.003

[6] Tsuda, Y., Saiki, T., Terui, F., et al. (2020): Hayabusa 2 mission status: landing, roving, and cratering on asteroid Ryugu, *Acta Astronautica* 171, pp. 42–54. DOI: 10.1016/j.actaastro.2020.02.035

[7] NASA, OSIRIS-REx (2022), https://solarsystem.nasa.gov/missions/osiris-rex/in-depth/ (last accessed Aug. 20, 2023)

[8] NASA, Double Asteroid Redirection Test (DART) (2022), https://solarsystem.nasa.gov/missions/dart/in-depth/ (last accessed Aug. 20, 2023)

[9] Sánchez, J.P., Yárnoz García, D. (2016): Asteroid retrieval missions enabled by invariant manifold dynamics, *Acta Astronautica* 127, 667-677. DOI: 10.1016/j.actaastro.2016.05.034

[10] Strange, N., Asphaug, E., Grogan, K., et al. (2010): Planetary Science Decadal Survey - Near-Earth Asteroid Trajectory Opportunities in 2020–2024, Jet Propulsion Laboratory, California Institute of Technology

[11] Landau, D., Dankanich, J., Strange, N., et al. (2013): Trajectories to NAB a NEA (near-Earth asteroid), AAS/AIAA Spaceflight Mechanics Meeting, February 10-14, Kauai (HI) Paper AAS 13-409

[12] Santos, D. P. S., Prado, A.F.B.A., Casalino, L., Colasurdo, G. (2008): Optimal trajectories towards near-earth-objects using solar electric propulsion (SEP) and gravity assisted maneuver, *Journal of Aerospace Engineering Sciences and Applications* pp. 51-64. DOI: 10.7446/jaesa.0102.06

[13] Abell, Barbee, Mink et al. (2012): The Near-Earth Object Human Spaceflight Accesslble Targets Study (NHATS) list of Near-Earth Asteroids: Identifying Potential Targets for Future Exploration, 43rd Lunar and Planetary Science Conference, March 19-23, The Woodlands (TX) Paper 2842.

[14] Fantino, E., Castelli, R. (2017): Efficient design of direct low-energy transfers in multi-moon systems, Celestial Mechanics & Dynamical Astronomy 127, 429-450, DOI: 10.1007/s10569-016-9733

[15] Canales, D., Howell, K. C., Fantino, E. (2021): Transfer design between neighborhoods of planetary moons in the circular restricted three-body problem: the moon-to-moon analytical transfer method, *Celestial Mechanics and Dynamical Astronomy* 133, 36, DOI: 10.1007/s10569-021- 10031-x

[16] Szebeheli, V. (1967): Theory of Orbits, Academic Press, New York. ISBN 978-0-12-395732-0

[17] Parker TS, Chua L. (1989): Practical numerical algorithms for chaotic systems. Springer-Verlag, New York, Berlin, Heidelberg. ISBN 0-387-96689-7

[18] NASA JPL, Astrodynamic Parameters, https://ssd.jpl.nasa.gov/astro_par.html (last accessed 25 Aug. 2023)

[19] NASA JPL, Small Bodies Database Query, https://ssd.jpl.nasa.gov/tools/sbdb_query.html (last accessed 25 Aug. 2023)

[20] Wen, W.L.S. (1961): A study of cotangential, elliptical transfer orbits in space flight, *Journal of Aerospace Sciences* 28(5), 411–417. DOI: 10.2514/8.9010

[21] Canales, D., Howell, K. C., Fantino, E. (2022): A versatile moon-to-moon transfer design method for applications involving libration point orbits, *Acta Astronautica* 198, 388-402, DOI: 10.1016/j.actaastro.2022.06.010.

[22] Canales, D., Howell, K.C., Fantino, E., Gilliam, A.J. (2023): Transfers between moons with escape and capture patterns via Lyapunov exponent maps, *Journal of Guidance, Control, and Dynamics*, in press. DOI: 10.2514/1.G007195